Articles

Computer Modeling of Nucleation, Growth, and Templating in Hydrothermal Synthesis

C. Richard A. Catlow* and David S. Coombes

Davy Faraday Research Laboratory, The Royal Institution, 21 Albemarle Street, London W1X 4BS, U.K.

Dewi W. Lewis

Department of Materials Science and Metallurgy, University of Cambridge, Pembroke Street, Cambridge CB2 3QZ, U.K.

J. Carlos G. Pereira

Departamento de Engenharia de Materiais, Instituto Superior Tecnico, Lisboa, Portugal

Received April 22, 1998. Revised Manuscript Received July 23, 1998

We examine the fundamental processes involved in the hydrothermal synthesis of silicates, using a range of computational techniques. We report ab initio calculations of the structures and energies of silica fragments. We estimate hydration energies by using both molecular mechanics methodologies and dielectric screening techniques. Detailed molecular mechanics calculations are reported for the interactions between solvated fragments of zeolitic structures and template molecules, emphasizing the role of the template in modifying fragments so that their structures are closer to those observed in zeolite crystals.

1. Introduction

Hydrothermal synthesis is a core technology in inorganic materials science. Hydrothermal methods are employed in the synthesis of microporous and mesoporous solids and, more generally, sol−gel procedures are widely used in syntheses of high-quality ceramic materials. An extensive range of empirical knowledge has accumulated about the factors controlling and optimizing such syntheses (see, e.g. Brinker and Scherer[1] and Barrer[2]). Understanding of the fundamental processes involved in the synthetic process is, however, sparse. The fundamental mechanisms are known to involve condensation and polymerization of precursor fragments in solution and, in the case of silicate systems, on which this paper concentrates, there is some knowledge (mainly from NMR[3,4]) of the nature of the precursor species in solution. Problems arise, however, in understanding the detailed role of organic templates, which are widely used as structure-directing agents in the synthesis of microporous solids.[5−7] Synthesis in templated systems is generally accepted to involve coordination of the silica species around the template in solution but, again, little detailed knowledge is available.

A considerable opportunity for advancing our understanding of these problems is provided by computer modeling techniques, whose rapid growth in recent years has made increasingly feasible the accurate calculation of molecular structures, energetics, dynamics, and reactivities. Modeling of hydration remains difficult, but again recent progress has made this key problem increasingly tractable.[8,9] In this paper, we describe recent applications of modeling techniques—both electronic structure methods and techniques based on interatomic potentials—to our understanding of the basic atomistic processes in gel chemistry, including the structures and energies of silica fragments, their interactions with water, and their condensation reactions. We then explore the interaction of such key fragments with simple organic templates, thereby allowing us to develop an understanding of the ways in which templates control the nucleation process. First, however,

* To whom correspondence should be addressed. Fax: 44-1-71-491-1501. E-mail: richard@ri.ac.uk.

(1) Brinker, C. J.; Scherer, G. W. *Sol−Gel Science, The Physics and Chemistry of Sol−Gel Processing*; Academic Press: New York, 1989.
(2) Barrer, R. M. *Hydrothermal Chemistry of Zeolites*; Academic Press: London, 1982.
(3) Engelhardt, G.; Michel, D. *High Resolution Solid State NMR of Silicates and Zeolites*; Wiley: New York, 1987.
(4) Harris, R. K.; Knight, C. T. G.; Hull, W. E. *J. Am. Chem. Soc.* **1981**, *103*, 1577.
(5) Lok, B. M.; Cannan, T. R.; Messina, C. A. *Zeolites* **1983**, *3*, 282.
(6) Gies, H.; Marler, B. *Zeolites* **1992**, *12*, 42.
(7) Davis, M. E.; Lobo, R. F. *Chem. Mater.* **1992**, *4*, 756.
(8) Smith, P. E.; Pettit, B. M. *J. Phys. Chem.* **1994**, *98*, 9700.
(9) Klamt, A.; Schüürmann, G. *J. Chem. Soc. Perkin Trans. 2* **1993**, 799.

10.1021/cm980302o CCC: $15.00
Published on Web 10/24/1998

we give a brief summary of the principle computational methodologies used.

2. Techniques

The methods used are standard so the account presented here is brief. Electronic structure methods employing density functional theory (DFT) are used to model the structures and energies of silica clusters. A variety of density functionals (DFs) and basis sets were used, as will be described in greater detail later. All DFT calculations used the DMOL code.[10] In a few of cases, calculations using based on Hartree−Fock (HF) methods were performed with the GAUSSIAN94 program.[11] Full geometric optimization was undertaken in all cases.

To model the interaction of the silicate clusters with water, we used both molecular mechanics (MM) and dynamics methods. As described in greater detail later, the clusters were represented by a modified version of the standard cvff MM potential;[12] cvff parameters were also used in modeling the cluster−water interactions. To model hydration, we first relaxed the clusters to equilibrium and then surrounded them with a sheath of water molecules. Full minimization of the cluster−water complex was then undertaken, followed in several cases by molecular dynamics and subsequent minimization; the latter procedure was used to help avoid local minima. The calculations were performed with the INSIGHT II/DISCOVER suite of MSI[12,13] and will be described further later.

3. Gel Chemistry

Our first objective is to gain a more detailed understanding of the structures and energies of key silica clusters and of the energetics and mechanisms of their condensation. Calculations are reported first on clusters in vacuo. Inclusion of the effect of hydration is, however, a crucial feature of our work and is reported later in this section.

The properties of silica clusters have been studied previously by both experimental and theoretical methods. In the last 10 years, extensive studies of silica species in solution have been made, using ^{29}Si NMR, liquid chromatography, vibrational spectroscopy, electron paramagnetic resonance, and other experimental techniques.[14−20] ^{29}Si NMR spectroscopy has been particularly effective in identifying the concentration and gross structural features of such clusters.[21−26] However, partly because so many different clusters are present in solution, it is difficult to study their properties individually by experimental techniques. As noted, however, recent developments in theoretical methods have made it possible to calculate the structures, energetics, and reactions of silica clusters with improved accuracy. Previous theoretical work includes semiempirical,[27,28] HF,[29−35] and DF calculations,[36−40] as well as molecular dynamics simulations.[41−43]

We now discuss the results of recent ab initio calculations on the silica clusters, which we compare, where possible, with available experimental data. Different DFs, both local (BHL) and nonlocal (BLYP), with double and the richer triple numerical basis sets with polarization (DNP and TNP, respectively) were used. We discuss all $Si_xO_y(OH)_z$ clusters with a maximum of five silicon atoms, plus some larger clusters, including the six-silicon ring and the eight-silicon cube. We consider first the open, noncyclic clusters, then the clusters with a ring, and finally the clusters with at least two rings. We present the most-relevant conformations for each cluster and analyze the corresponding energetic and

(10) DMOL[3]; Molecular Simulations, Inc.: San Diego, 1997.
(11) Frisch, M. J.; Trucks, G. W.; Schlegel, H. B.; Gill, P. M. W.; Johnson, B. G.; Robb, M. A.; Cheeseman, J. R.; Keith, T.; Petersson, G. A.; Montgomery, J. A.; Raghavachari, K.; Al-Laham, M. A.; Zakrzewski, V. G.; Ortiz, J. V.; Foresman, J. B.; Cioslowski, J.; Stefanov, B. B.; Nanayakkara, A.; Challacombe, M.; Peng, C. Y.; Ayala, P. Y.; Chen, W.; Wong, M. W.; Andres, J. L.; Replogle, E. S.; Gomperts, R.; Martin, R. L.; Fox, D. J.; Binkley, J. S.; Defrees, D. J.; Baker, J.; Stewart, J. J. P.; Head-Gordon, M.; Gonzales, C.; Pople, J. A. *Gaussian94*; Gaussian, Inc.: Pittsburgh, 1995.
(12) INSIGHT II, 400 ed.; Moleular Simulations, Inc.: San Diego, 1996.
(13) Discover, 400 ed.; Molecular Simulations, Inc.: San Diego, 1996.
(14) Keefer, K. D. In *Better Ceramics through Chemistry*; Brinker, C. J., Clark, D. E.; Ulrich, D. R., Eds.; Materials Research Society, Elsevier Science Publishing Co.: New York, 1984; Vol. 32, p 15.
(15) Orcel, G.; Hench, L. *J. Non-Cryst. Solids* **1986**, *79*, 177.
(16) Balfe, C. A.; Martinez, S. L. In *Better Ceramics through Chemistry II*; Brinker, C. J., Clark, D. E., Ulrich, D. R., Eds.; Materials Research Society, Elsevier Science Publishing Co.: New York, 1986; Vol. 73, p 27.
(17) Pouxviel, J. C.; Boilot, J. P. *J. Non-Cryst. Solids* **1987**, *94*, 374.
(18) Tallant, D. R.; Bunker, B. C.; Brinker, C. J.; Balfe, C. A. In *Better Ceramics through Chemistry II*; Brinker, C. J., Clark, D. E., Ulrich, D. R., Eds.; Materials Research Society, Elsevier Science Publishing Co.: New York, 1986; Vol. 73, p 261.
(19) Kinrade, S. D.; Swaddle, T. W. *Inorg. Chem.* **1988**, *27*, 4253.
(20) Jonas, J. In *Ultrastructure Processing of Advanced Materials*; Uhlmann, D. R., Ulrich, D. R., Eds.; John Wiley & Sons, Inc.: New York, 1992; p 13.
(21) Klemperer, W. G.; Mainz, V. V.; Millar, D. M. In *Better Ceramics through Chemistry II*; Brinker, C. J., Clark, D. E., Ulrich, D. R., Eds.; Materials Research Society, Elsevier Science Publishing Co.: New York, 1986; Vol. 73, p 3.
(22) Klemperer, W. G.; Mainz, V. V.; Millar, D. M. In *Better Ceramics through Chemistry II*; Brinker, C. J., Clark, D. E., Ulrich, D. R., Eds.; Materials Research Society, Elsevier Science Publishing Co.: New York, 1986; Vol. 73, p 15.
(23) Klemperer, W. G.; Ramamurthi, S. D. In *Better Ceramics through Chemistry III*; Brinker, C. J., Clark, D. E., Ulrich, D. R., Eds.; Materials Research Society, Elsevier Science Publishing Co.: New York, 1988; Vol. 121, p 1.
(24) Klemperer, W. G.; Mainz, V. V.; Ramamurthi, S. D.; Rosenberg, F. S. In *Better Ceramics through Chemistry III*; Brinker, C. J., Clark, D. E., Ulrich, D. R., Eds.; Research Society, Elsevier Science Publishing Co.: New York, 1988; Vol. 121, p 15.
(25) Knight, C. T. G. *Zeolites* **1990**, *10*, 140.
(26) Kelts, L. W.; Armstrong, N. J. *J. Mater. Res.* 1989, 4, 423.
(27) West, J. K.; Zhu, B. F.; Cheng, Y. C.; Hench, L. L. *J. Non-Cryst. Solids* **1990**, *121*, 51.
(28) West, J. K.; Wallace, S.; Hench, L. L.; Lishawa, C. R. In *Ultrastructure Processing of Advanced Materials*; Uhlmann, D. R., Ulrich, D. R., Eds.; John Wiley & Sons: New York, 1992; p 111.
(29) Lasaga, A. C.; Gibbs, G. V. *Phys. Chem. Miner.* **1987**, *14*, 107.
(30) Lasaga, A. C.; Gibbs, G. V. *Phys. Chem. Miner.* **1988**, *14*, 29.
(31) Ahlrichs, R.; Bär, M.; Häser, M.; Kölmel, C.; Sauer, J. *Chem. Phys. Lett.* **1989**, *164*, 199.
(32) Sauer, J. *Chem. Rev.* **1989**, *89*, 199.
(33) Hill, J.-R.; Sauer, J. *J. Phys. Chem.* **1994**, *98*, 1238.
(34) Gibbs, G. V.; Downs, J. W.; Boisen, M. B. *Rev. Miner.* **1994**, *29*, 331.
(35) Moravetski, V.; Hill, J.-R.; Eichler, U.; Cheetham, A. K.; Sauer, J. *J. Am. Chem. Soc.* **1996**, *118*, 13015.
(36) Stave, M. S.; Nicholas, J. B. *J. Phys. Chem.* **1993**, *97*, 9630.
(37) Pápai, I.; Goursot, A.; Fajula, F.; Weber, J. *J. Phys. Chem.* **1994**, *98*, 4654.
(38) Sierka, M.; Sauer, J. *J. Chem. Soc. Faraday Discuss.* **1997**, *106*, 41.
(39) Pereira, J. C. G.; Catlow, C. R. A.; Price, G. D. Manuscript submitted.
(40) Pereira, J. C. G.; Catlow, C. R. A.; Price, G. D. Manuscript submitted.
(41) Feuston, B. P.; Garofalini, S. H. *J. Chem. Phys.* **1988**, *89*, 5818.
(42) Feuston, B. P.; Garofalini, S. H. *J. Phys. Chem.* **1990**, *94*, 5351.
(43) Garofalini, S. H.; Martin, G. *J. Phys. Chem.* **1994**, *98*, 1311.

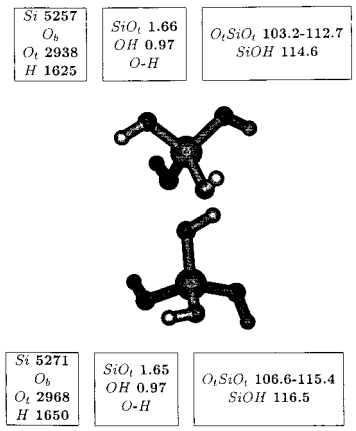

Figure 1. Bond lengths (Å), bond angles (deg), and Hirshfeld atomic charges (0. and minus sign in O charges are omitted) for D_{2d} (top) and S_4 $Si(OH)_4$ conformations, optimized at the DF−BLYP/TNP level of approximation.

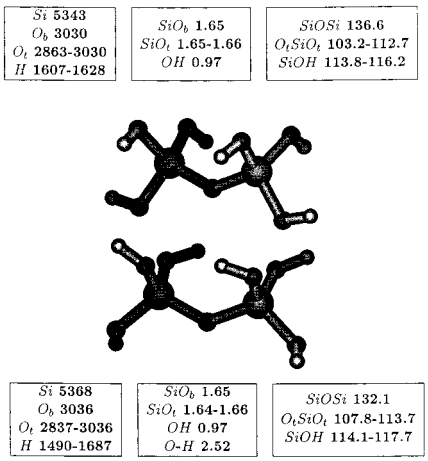

Figure 2. Bond lengths (Å), bond angles (deg), and Hirshfeld atomic charges for C_{2v} (top) and C_2 $Si_2O(OH)_6$ conformations, optimized at the DF−BLYP/TNP level of approximation.

structural details. Our study, which represents the first detailed conformational analysis of the clusters, demonstrates that hydrogen bonding exerts a critical influence on the conformations calculated. Complex silica clusters are classified according to the NMR notation, Q_n^m, where n represents the number of silicons that are bonded to m bridging oxygens. When this notation is insufficient, we use e and c, for edge and corner, and cis and trans specifications, respectively.

3.1. Open Clusters. The cluster structures considered under this heading vary from the simple monomer and dimer to linear and branched structures that contain five silicon atoms.

3.1.1. Monomer and Dimer: Intramolecular Effects. The monomer and dimer are the most studied silica clusters. In the gas phase, the condensation reaction energy depends considerably on the strength of the hydrogen bonds in the dimer.

In the case of $Si(OH)_4$, two conformations are relevant, those with point symmetry D_{2d} and S_4. The S_4 conformation is the global minimum in the gas phase, and the D_{2d} is a local minimum. The structure and charge distribution for both conformations are presented in Figure 1. These calculations utilize the BLYP DF with a high-quality TNP basis set. The energy difference between the two conformations is calculated as 1.8 kcal mol^{-1}. Sauer[32] reported a slightly higher value for this energy difference: 3.2 kcal mol^{-1} at the HF/6−31G** level. At the DF−BLYP/TNP level, the OSiO angles match exactly the reference HF values,[32] whereas the SiOH angle is 2.3° smaller and the SiO and OH bond lengths are only 0.02 and 0.03 Å, respectively, larger than in the HF study. The distance between adjacent hydroxyl groups is too large to allow the formation of hydrogen bonds.

The conformations for the dimer, that is, the $Si_2O(OH)_6$ cluster, with the lowest energy and the highest symmetry (C_2 and C_{2v}, respectively) are presented in Figure 2, for the DF−BLYP/TNP level of approximation. At this level, the C_2 conformation is +5.7 kcal mol^{-1} more stable than the C_{2v}. This energy difference is substantial and shows the importance of these conformational analyses.

The calculated condensation energies required to form the dimer from the monomer, as in 2 $Si(OH)_4 \rightarrow Si_2O(OH)_6 + H_2O$, for the lowest-energy conformations are presented in Table 1. At the DF−BHL/DNP level of approximation, the energy is calculated as −9.4 kcal mol^{-1}, but the value decreases to −2.8 kcal mol^{-1} at the DF−BLYP/DNP level and decreases further, to −2.2 kcal mol^{-1}, at the DF−BLYP/TNP level. Two hydrogen bonds present in $Si_2O(OH)_6$ are not present in the $Si(OH)_4$ reactants, and the simpler BHL/DNP procedure is known to exaggerate the hydrogen bonding energies. As in the water dimer (see Table 1), the MP2 prediction (−7.8 kcal mol^{-1}) is smaller than the local DF−BHL/DNP calculation but higher than the best nonlocal DF−BLYP/TNP calculation. Assuming that the difference in energy between local and nonlocal density calculations is due only to the two intramolecular hydrogen bonds occurring in $Si_2O(OH)_6$, we estimate the error per hydrogen bond committed in DF−BHL/DNP calculations to be ∼−3.3 kcal mol^{-1}, close to the corresponding error in the water dimer, (−4.7 kcal mol^{-1}). The difference between the two values is probably attributable to the SiOSi angle requirements, which force the hydrogen bonds to be longer than in the water dimer. At the DF−BLYP/TNP level, the SiOSi angle is calculated as 132.1°, which appears reasonable, although no experimental results are available for $Si_2O(OH)_6$ in vacuo. We will use the correction of 3.3 kcal mol^{-1} per hydrogen bond in later calculations on clusters that, owing to their size, were confined to analysis at the DF−BHL/DNP level. However, this approach depends on the corrections being additive and all the hydrogen bonding terms being equivalent. More rigorous determinations of energies and structures containing hydrogen bonds are now possible by using nonlocal DFs.

Table 1. $Si(OH)_4$ Condensation Energy (kcal mol^{-1}) and H_2O Dimerization Energy (kcal mol^{-1}) after ab initio Optimization

method	silica condensation	water dimerization
DF−BHL/DNP	−9.4	−11.3
DF−BLYP/DNP	−2.8	−6.4
DF−BLYP/TNP	−2.2	−4.3
HF/6−31G**	−7.8[a]	−7.1

[a] From Sauer.[32]

3.1.2. Linear Trimer, Tetramer, and Pentamer: Effects of Ring Formation. We now analyze the linear noncyclic clusters, that contain three, four, or five

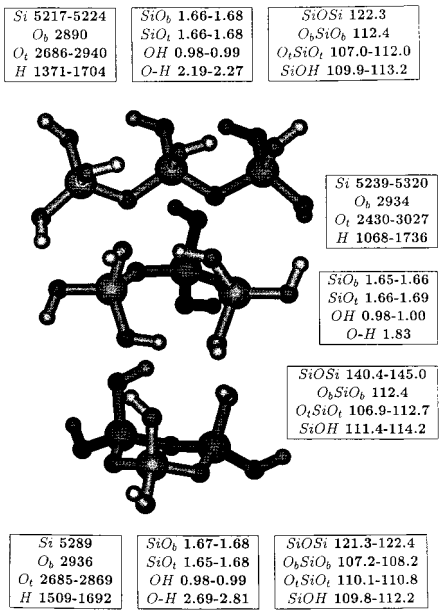

Figure 3. Bond lengths (Å), bond angles (deg), and Hirshfeld atomic charges for $Si_3O_2(OH)_8$ conformations forming $Si_3O_3(OH)_6$, optimized at the DF−BLYP/DNP level of approximation.

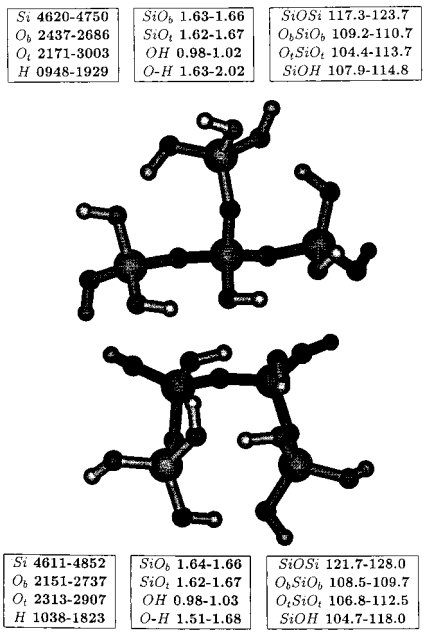

Figure 4. Bond lengths (Å), bond angles (deg), and Hirshfeld atomic charges for noncyclic four-silicon clusters, optimized at the DF−BHL/DNP level of approximation.

silicon atoms. These clusters can form curved, almost cyclic structures, which can react to form the rings observed experimentally.

Linear Trimer. The linear trimer and the trimer ring are the largest silicate clusters we studied with nonlocal DFs. At the DF−BLYP/DNP level of approximation, the lowest energy conformation found for the linear trimer is almost cyclic, with two hydrogen bonds closing the ring. This conformation is 2.2 kcal mol^{-1} more stable than the straight one, where the chain ends are far apart. The structure and charge distribution for both conformations are shown in Figure 3.

The almost cyclic conformation may, in turn, be transformed into the trimer ring by an intramolecular condensation reaction. The corresponding energy, though positive, is sufficiently small (+13.2 kcal mol^{-1}) to explain how a relatively strained cluster such as the 3-silicon ring may be formed.

The hydrogen bonds are overestimated at the DF−BHL/DNP level of approximation, because the O···H distances are too small (∼1.64 Å) and the OH bond lengths in the acceptor groups are too large (1.02 Å). The condensation energy at the DF−BHL/DNP level (−18.5 kcal mol^{-1}) is too high compared with the results for the dimer. Applying the energy difference discussed above, between local and nonlocal DF found for the dimer (3.3 kcal mol^{-1} per overestimated hydrogen bond), we recalculated the condensation energy as −11.9 kcal mol^{-1}. At the DF−BLYP/DNP level, the condensation energy becomes −7.7 kcal mol^{-1}, smaller than even the corrected DF−BHL/DNP value. For this, or larger clusters with hydrogen bonds, which at the moment can be studied only at the DF−BHL/DNP level, even the corrected values should be considered as an upper limit for the actual results. At the DF−BLYP/DNP level, the O···H and OH bond lengths, 1.83 and 1.00 Å, respectively, are close to the expected values. Recent HF work for this cluster has been reported by Ferrari et al.,[44] using SiH_3 instead of $Si(OH)_3$ terminal groups, and by Hill and Sauer,[33] using symmetry constraints.

Linear Tetramer. As in the linear trimer, the lowest-energy conformation found for the linear tetramer is almost cyclic, with hydrogen bonds linking the chain ends. At the DF−BHL/DNP level of approximation, this curved conformation is 11.6 kcal mol^{-1} more stable than the straight conformation. The structure and charge distribution for the lowest-energy conformations are presented in Figure 4. The five hydrogen bonds in the curved conformation have an O···H distance that is too short (1.51−1.68 Å) and an OH distance that is too large (1.01−1.05 Å); the six hydrogen bonds in the straight conformation are much weaker.

Although the effect of improving the level of approximation is not clear, we would reasonably expect that the curved conformation is still highly probable, in agreement with the experimental evidence, which shows that it is relatively easy to produce four-silicon rings. The easiest way to form a four-silicon ring is probably to close an open four-silicon linear chain, which should be particularly simple when starting from this almost cyclic conformation.

The total condensation energy for the curved conformation (−38.2 kcal mol^{-1}) again appears to be too large when compared with the best dimer calculations. Applying the correction factor previously estimated for each overestimated hydrogen bond, the corrected condensation energy for the most-stable conformation is −21.7 kcal mol^{-1}. Again, we consider that this value might still be too negative.

Linear Pentamer. The lowest-energy conformation found for the linear pentamer is again almost cyclic, with four hydrogen bonds closing three secondary rings. At the DF−BHL/DNP level, this conformation is 11.4

(44) Ferrari, A. M.; Ugliengo, P.; Garrone, E. *J. Phys. Chem.* **1993**, *97*, 2671.

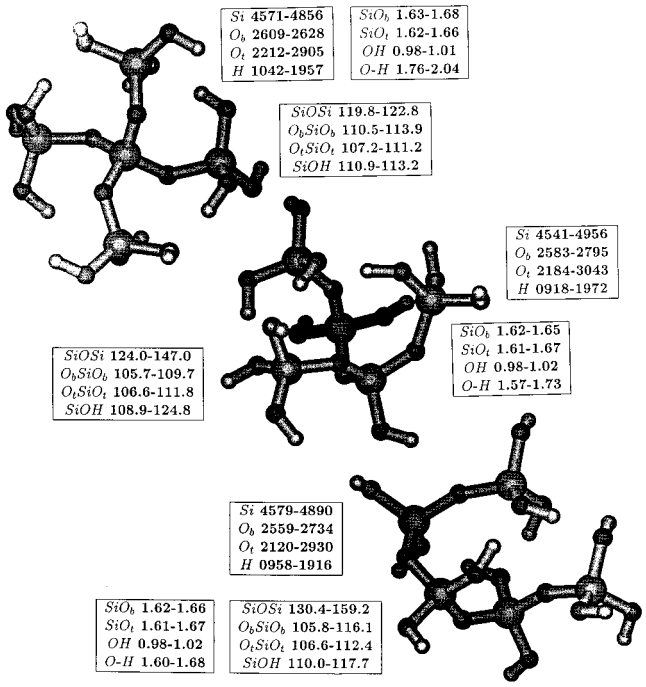

Figure 5. Bond lengths (Å), bond angles (deg), and Hirshfeld atomic charges for noncyclic five-silicon clusters, optimized at the DF−BHL/DNP level of approximation.

kcal mol^{-1} more stable than the straight conformation. The structure and charge distribution for the lowest-energy conformation are presented in Figure 5.

The total condensation energy for the curved conformation is substantially negative (−43.6 kcal mol^{-1}). Even after correcting the energy to account for the overestimation of the four hydrogen bonds, the condensation energy is only 1.8 kcal mol^{-1} less than calculated for the uncorrected straight conformation. Therefore, at higher levels of approximation, the almost cyclic conformation should remain highly stable.

This conformation is remarkable because it allows the subsequent formation of several different clusters through a single intramolecular condensation reaction. If each of the four oxygen atoms bonded to hydrogens in different silicons (see Figure 5, bottom) instead react directly with these in a nucleophilic attack, the five-silicon ring, the branched four-silicon ring, the branched three-silicon ring, and the double-branched three-silicon ring can all be formed. The pentamer, straight conformation, with weaker hydrogen bonds (O···H of 1.94−2.13 Å), presents intermediate values for the SiO and OH bond lengths and relatively small SiOH angles (<113.5°), because of the directionality of the hydrogen bonds.

3.1.3. Branched Tetramer and Pentamer Clusters: Branching Effects. In this section, we analyze the branched noncyclic clusters containing four and five silicon atoms. We find that the branched clusters have higher energies than the linear clusters and should therefore be less stable, in agreement with experimental findings.

Branched Four-Silicon Cluster. The structure and charge distribution of the noncyclic four-silicon clusters are presented in Figure 4. The proposed conformation for the branched tetramer (above, in Figure 4) has four hydrogen bonds: two with a reasonable O···H distance (1.80 and 2.02 Å) and the other two being too short (1.63−1.64 Å).

Although the condensation energy for the branched tetramer is considerably negative (−30.6 kcal mol^{-1}), it is 7.5 kcal mol^{-1} less favorable than for the linear cluster. This result is in agreement with the experimental evidence, which shows that it is much easier to form the linear than the branched tetramer.[23] However, because the linear tetramer has five apparently overestimated hydrogen bonds against only two in the branched tetramer, applying the correction of 3.3 kcal mol^{-1} per hydrogen bond makes the energy lower for the branched cluster (−24.0 kcal mol^{-1}) than for the linear cluster (−21.7 kcal mol^{-1}). The correction made here may therefore be exaggerating the relative stability of the branched structure, but the two types of cluster probably have similar energies.

Branched Five-Silicon Cluster. The structure and charge distribution of the noncyclic five-silicon clusters are also presented in Figure 5. The most stable conformation found for the branched five-silicon cluster (Figure 5, center) has four hydrogen bonds, which are probably too short (O···H = 1.64−1.72 Å), and forms three secondary rings. The condensation energy (−40.2 kcal mol^{-1}) is 3.4 kcal mol^{-1} less than for the linear chain, decreasing to −27.0 kcal mol^{-1} when corrected for the hydrogen bonds (compared with −30.4 kcal mol^{-1} for the corrected linear chain). The corrected energy is probably a reasonable estimate, compared with the values obtained for the previous clusters.

Five-Silicon Cross. In the pentamer cross (Figure 5, top), a central silicon is attached to four bridging oxygens, each of which is subsequently bonded to a terminal $Si(OH)_3$, forming a highly symmetric structure. The best conformation found for this cluster has six hydrogen bonds, forming several secondary rings. The cluster is therefore a good precursor to produce the double-branched three-silicon ring by forming an intramolecular SiOSi disiloxane bond.

The condensation energy for the pentamer cross, though relatively large (−32.0 kcal mol^{-1}), is still 8.2 kcal mol^{-1} less than for the branched chain (−40.2 kcal mol^{-1}). Taking into account the three overestimated hydrogen bonds, the corrected energy is −22.1 kcal mol^{-1}, less than the corrected energy (−27.0 kcal mol^{-1}) for the branched pentamer. Because the condensation energy for the branched pentamer is, in turn, less than for the linear chain, at the local density approximation (LDA) level, the cluster stability apparently decreases with the degree of branching, in agreement with the experimental evidence.[23] We note that this cluster was also investigated by Lasaga and Gibbs,[30] who used potentials derived from 6−31G* calculations for the monomer and dimer.

The pentamer cross is the only cluster discussed in this review in which a silicon atom is bonded to four unconstrained bridging oxygens (O_b). The central SiO_b bonds are slightly shorter (1.63−1.64 Å) than the adjacent O_bSi bonds (1.64−1.68 Å), although this difference is relatively small. This finding agrees with the experimental and theoretical evidence that the SiO bond length tends to decrease in more-bridged systems. The SiO bond length in α-quartz, for instance (1.60 Å[45]), is

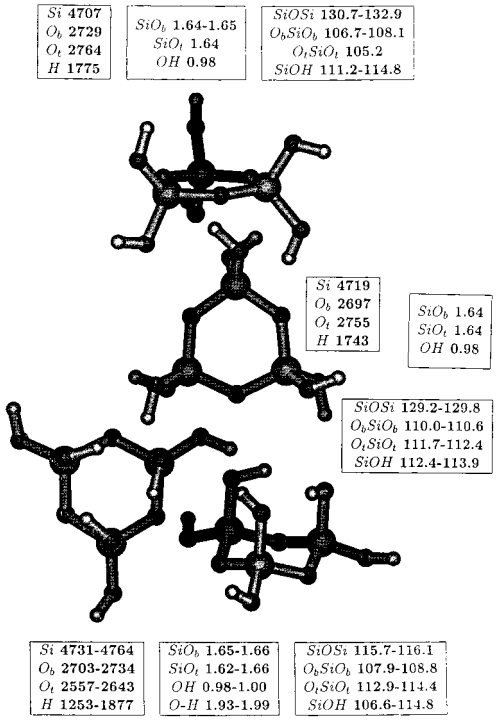

Figure 6. Bond lengths (Å), bond angles (deg), and Hirshfeld atomic charges for $Si_3O_3(OH)_6$ conformations, optimized at the DF−BHL/DNP level of approximation.

shorter than the predicted value for $Si(OH)_4$ in the gas phase (∼1.62 Å[32]).

3.2. Clusters Containing a Single Ring. In our discussion of these clusters, we consider first the trimer and tetramer rings, which have particularly relevant conformations; the branched trimer and tetramer rings, with a lateral chain containing one silicon atom; the trimer rings containing two silicon atoms in lateral chains; and finally, the larger five- and six-silicon rings.

3.2.1. Trimer and Tetramer Rings: Ring Conformations. In this section, we analyze the smallest silica rings, presenting the most relevant conformations. Trimer and tetramer rings in vacuo are strongly stabilized by an intramolecular cyclic hydrogen bond system.

Trimer Ring. Figure 6 shows the three most-relevant conformations found in this work for the cyclic trimer. At the DF−BHL/DNP level of approximation, the bottom conformation (in Figure 6) is 5.3 kcal mol^{-1} more stable than the middle configuration, which in turn is 0.8 kcal mol^{-1} more stable than the upper configuration.

The lowest-energy conformation has a chair conformation (as in six-carbon rings), in which three hydroxyl groups occupy equatorial positions and the other three are disposed in axial positions, forming a strong system of three hydrogen bonds. At this level of approximation, the total energy of condensation is still exothermic (−1.6 kcal mol^{-1}), despite the strain associated with this ring. At the DF−BLYP/DNP level of approximation, the total condensation energy is already positive but still small (+5.5 kcal mol^{-1}), so this conformation should be present in silica solutions, despite its internal strain, as shown experimentally for low pH.[25]

The SiOSi angle is much larger in the two planar rings than in the chair conformation (∼116.0°). The SiOH angle assumes two distinct values, one for the equatorial hydroxyl groups (∼114.5°, as in previous clusters), and another, much smaller one (∼106.8°) for the axial hydroxyl groups, which are constrained by the directionality of the hydrogen bonds. However, at the DF−BLYP/DNP level, the O···H distances are relatively long (2.69−3.01 Å).

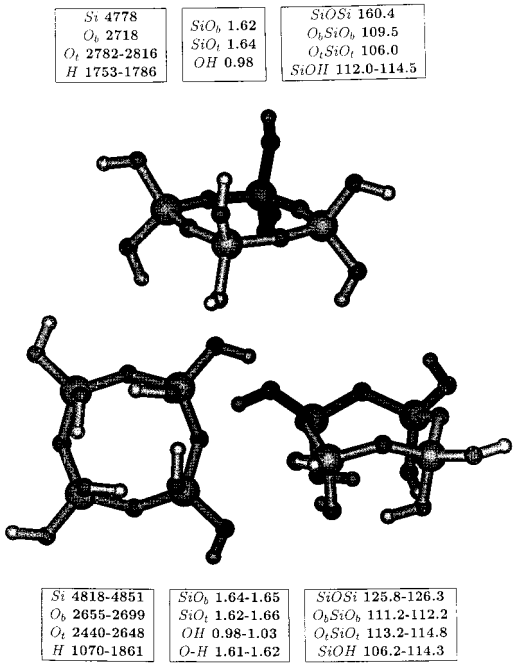

Figure 7. Bond lengths (Å), bond angles (deg), and Hirshfeld atomic charges for $Si_4O_4(OH)_8$ conformations, optimized at the DF−BHL/DNP level of approximation.

Tetramer Ring. The lowest-energy conformation found for the four-silicon ring is a crown conformation (also the most stable conformation in eight-carbon rings[46]), which decreases the ring strain and allows the formation of a strong cyclic system of four hydrogen bonds, decreasing considerably the energy of the cluster. At the DF−BHL/DNP level of approximation, this conformation is 31.9 kcal mol^{-1} more stable than a planar tetramer, which is more symmetric but has relatively weak hydrogen bond interactions. The structure and charge of both conformations are presented in Figure 7. The SiOSi angles are much larger (160.4°) in the planar conformation, reflecting the different atomic arrangements of the two rings. The SiOSi angle is larger in the four- than in the three-silicon ring.

Although the ring strain should be considerably less in this cluster than in the more-constrained trimer ring, the total condensation energy for the crown conformation (−25.7 kcal mol^{-1}) is very probably too negative, compared with the nonlocal density results obtained for the two- and three-silicon clusters, a result due essentially to the overestimation by the LDA method of the four hydrogen bonds, whose length is too small (∼1.62 Å). Correcting the energy according to the results for the dimer yields a condensation energy of −12.5 kcal mol^{-1}, which is much more acceptable. Other studies for this ring have been reported by Moravetski et al.,[35] Hill and Sauer,[33] and West et al.,[27] but only for the planar conformation.

(45) Kubicki, J. D.; Lasaga, A. C. *Am. Mineral.* **1988**, *73*, 941.

(46) Dunitz, J. D.; Ibers, J. A. *Perspectives in Structural Chemistry II*; John Wiley & Sons, Inc.: New York, 1968.

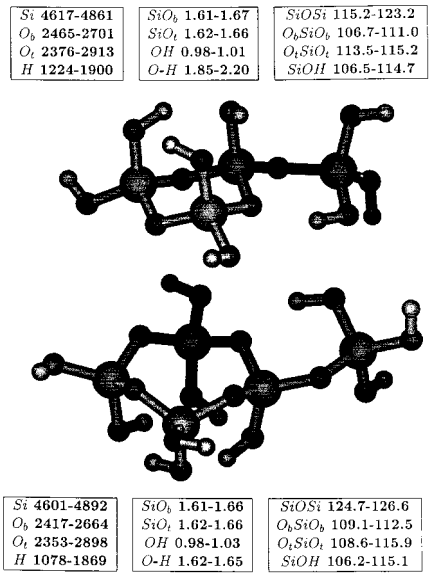

Figure 8. Bond lengths (Å), bond angles (deg), and Hirshfeld atomic charges for $Q_2^2\,Q_1^3\,Q_1^1$ and $Q_3^2\,Q_1^3\,Q_1^1$, optimized at the DF−BHL/DNP level of approximation.

3.2.2. Branched Rings: One-Silicon Branched Trimer and Tetramer Rings. We now analyze the simplest branched rings, the trimer and tetramer rings that contain a one-silicon lateral chain. Both clusters have a relatively negative condensation reaction energy (from the monomer) and keep the "chair" and "crown" conformations found for the nonbranched rings.

Branched Trimer Ring. The branched trimer and tetramer rings, are presented in Figure 8. The branched trimer ring (Figure 8, top) results from the association of a trimer ring (in a "chair" conformation) with a monomer (in an S_4 conformation), arranged in such a way that a bridging oxygen in the ring forms a hydrogen bond with the $Si(OH)_3$ chain. This hydrogen bond introduces a second link between the ring and the chain, in this way increasing considerably the rigidity of the cluster. This hydrogen bond is similar in strength (1.91 Å) to the three hydrogen bonds in the ring (O···H = 1.85−2.20 Å), which are slightly distorted by the influence of the lateral chain. The length of the SiO bond linking the ring and the chain is much shorter (1.61 Å) than the others in the ring or in the chain.

The condensation energy of −6.0 kcal mol^{-1} (i.e., 4.4 kcal mol^{-1} less than for the three-silicon ring), although relatively small, because of the ring strain is sufficiently negative to result in the significant concentration of this cluster usually found in sol−gel solutions.[25,26]

Branched Tetramer Ring. The branched tetramer ring (see Figure 8, bottom) is formed by associating a tetramer ring (in a crown conformation) with an S_4 monomer, thus preserving most of the features of these clusters. The lateral chain adds a further hydrogen bond (O···H = 1.96 Å) to the four hydrogen bonds in the ring (O···H = 1.62−1.65 Å), thus considerably increasing the rigidity of the cluster because the lateral chain cannot rotate any more. The SiO bond length is shorter (1.62 Å) than in open chains.

The condensation energy for this cluster of −31.0 kcal mol^{-1} (i.e., 5.3 kcal mol^{-1} less than for the four-silicon ring) is considerably negative because of the five hydrogen bonds. When corrected for the four overestimated hydrogen bonds, the energy is estimated as −17.8 kcal mol^{-1}.

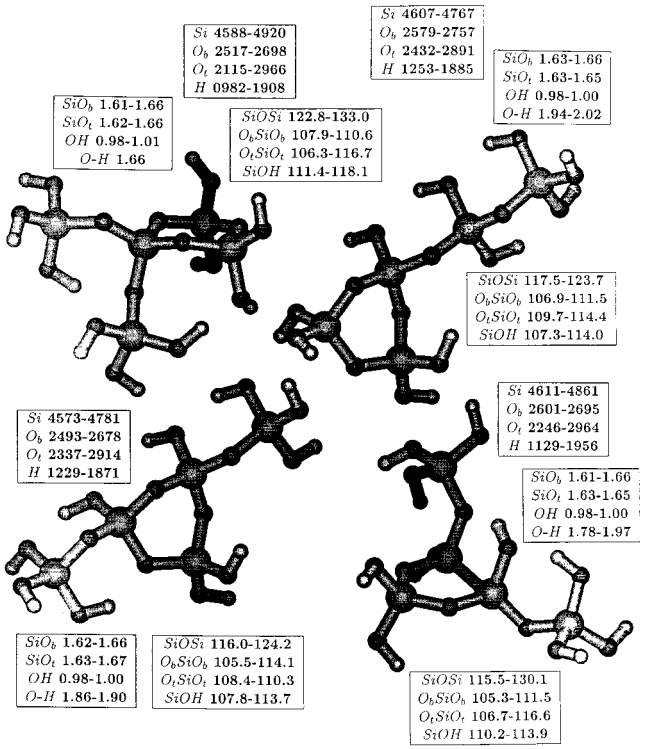

Figure 9. Bond lengths (Å), bond angles (deg), and Hirshfeld atomic charges for $Q_2^2\,Q_1^3\,Q_1^2\,Q_1^1$, $Q_2^2\,Q_1^2\,Q_1^4$, $Q_2^3\,Q_2^1\,Q_1^2$cis, and $Q_2^3\,Q_2^1\,Q_1^2$trans, optimized at the DF−BHL/DNP level of approximation.

3.2.3. Branched Rings: Two-Silicon Branched Trimer Rings. We now analyze the four trimer rings containing two silicon atoms in lateral chains. These clusters have similar energies and structural features and should be slightly more stable than the trimer ring.

Single-Branched Trimer Ring. The trimer rings with two silicon atoms in lateral chains are presented in Figure 9. The trimer ring with a single two-silicon chain (Figure 9, top right) is formed by associating the ring (in the "chair" conformation) with a dimer (in the C_2 conformation), arranged to allow the formation of three hydrogen bonds (two in the lateral chain and one between the chain and the ring), increasing considerably the rigidity of the cluster. The corresponding O···H distances are reasonable (1.94−2.02 Å), so the calculated condensation energy (−10.95 kcal mol^{-1}) is probably accurate enough not to need any correction.

trans-Branched Trimer Ring. In the trans-branched trimer ring (bottom right, Figure 9), two lateral chains with one silicon each are attached to different silicons on different sides of the ring. The three hydrogen bonds in this cluster are apparently too strong in calculations at the LDA level. However, the differences between the various hydroxyl groups are smaller than in previous clusters.

The condensation energy for this cluster (−10.5 kcal mol^{-1}) is only 0.5 kcal mol^{-1} more than in the previous cluster, but the difference increases (to −7.2 kcal mol^{-1}) after correcting the energy to take into account one possibly overestimated hydrogen bond.

cis-Branched Trimer Ring. The cis-branched trimer ring (bottom left, Figure 9) differs from the previous

cluster because the two lateral chains are on the same side of the ring, forming three hydrogen bonds with reasonable bond lengths (O···H = 1.86−1.90 Å) and a fourth that is very weak (O···H = 2.74 Å).

The condensation energy for the cis-branched cluster (−10.95 kcal mol^{-1}) is almost identical to the energy calculated for the trans-branched cluster and matches exactly the energy obtained for the trimer ring with a two-silicon chain, suggesting that from the energetic point of view the structural differences between these clusters are irrelevant. The trans-cluster becomes 3.8 kcal mol^{-1} less stable after correcting for its overestimated hydrogen bonds, although there is some uncertainty in the reliability of the correction in this case.

Double-Branched Trimer Ring. In the double-branched trimer ring (top left, Figure 9), two lateral chains are attached to the same silicon atom in the ring, forming two hydrogen bonds (O···H = 1.66 and 1.96 Å), the first of which is probably overestimated. The condensation energy (−11.3 kcal mol^{-1}) is calculated as roughly equal to or slightly more negative than in the three previous clusters, which is surprising, because only two hydrogen bonds exist in this conformation, compared with three in the previous clusters.

For all these clusters, the SiO_b bonds linking the chain with the ring is strong, with bond lengths of 1.61−1.64 Å. In compensation, the next SiO_b bonds in the chain are weaker, with bond lengths of 1.66−1.67 Å. These bonds are even longer than in the ring, a trend already noted for the one-silicon branched trimer ring. We also note that the range of variation of the SiOSi bond differs among the four clusters.

3.2.4. Larger Rings: Pentamer and Hexamer Rings. We now analyze the larger five- and six-silicon rings. Our results suggest that, in vacuo, the four- and six-silicon rings are more stabilized by strong hydrogen bond systems than is the five-silicon cluster, which lacks the required symmetry, even though ring strain factors influence the relative stabilities of the clusters.

Pentamer Ring. The five- and six-silicon rings are presented in Figure 10. The five-silicon ring has the *S* shape conformation usually proposed for 10-carbon rings,[46] but this *S* shape is distorted by four hydrogen bonds formed in this cluster. The hydrogen bond distortions in the five-silicon ring explain the large bond length variations in the bridging and terminal groups. The total condensation energy for the five-silicon ring (Figure 10, top) is less (−25.2 kcal mol^{-1}) than that for the four-silicon ring (−25.7 kcal mol^{-1}) because the symmetry of the former is much less and a cyclic hydrogen bond system is no longer present. However, the LDA-corrected energy (−18.5 kcal mol^{-1}) is less than the value obtained for the tetramer ring (−12.5 kcal mol^{-1}). The larger five-silicon ring allows a better relaxation of the ring strain, though stronger hydrogen bonds may be formed in the four-silicon ring, where the hydroxyl groups are closer to each other.

Hexamer Ring. The six-silicon ring (Figure 10, bottom) has an "extended crown" conformation, with six hydroxyl groups forming a cyclic hydrogen bond system that stabilizes the cluster enormously. The strength of these hydrogen bonds seem to be seriously overestimated, the O···H bond lengths (1.56−1.60 Å) being too short and the corresponding OH bond lengths (1.03−1.04 Å) too long. Consequently, the total condensation energy for the six-silicon ring (−48.7 kcal mol^{-1}) is likely to be overestimated. The corrected value (−28.9 kcal mol^{-1}) seems much more reasonable. In the six-silicon ring, the SiOSi angles (127.1−130.0°) are relatively similar to those in the four-silicon ring. The three-, four-, five-, and six-silicon rings discussed here have also been studied by Hill and Sauer,[33] using HF with double-zeta and triple-zeta with polarization (DZP and TZP) basis sets, but only for the planar conformations and with use of symmetry constraints. The corresponding condensation energies they report are more negative than the DF values presented here.

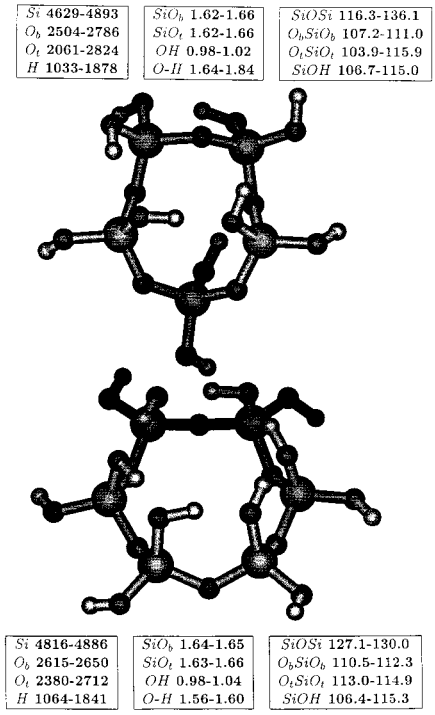

Figure 10. Bond lengths (Å), bond angles (deg), and Hirshfeld atomic charges for large rings, optimized at the DF−BHL/DNP level of approximation.

3.3. Multiple-Ring Clusters. Our analysis of the clusters containing several rings considers the trimer−trimer double rings, bonded by an edge; the trimer−trimer double ring, bonded by a corner, together with the two tetramer−trimer double rings; and finally the multiple rings: the octamer, the double-hexamer, and the sodalite cages.

3.3.1. Double Rings: Trimer−Trimer Rings. The double rings, with two intramolecular condensations, are the most-strained clusters studied in this work. In this section we analyze the double-trimer rings that share a common edge. Experimentally, these clusters are not usually observed.

Trimer−Trimer Ring. The structure and charge distribution for the clusters with two trimer rings bonded by an edge are presented in Figure 11. The four-silicon double ring (Figure 11, top), which is never found in sol−gel solutions,[24−26] is the least-stable cluster discussed in this work. Its substantial ring strain from the two rings (both with "chair" conformations) is increased by the additional constraint of sharing a common SiOSi edge. Furthermore, only a single hydrogen bond can be formed at a reasonable distance (2.0

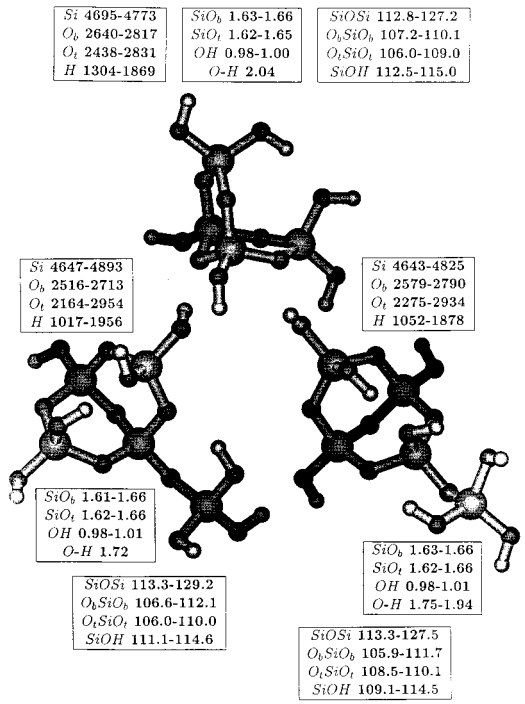

Figure 11. Bond lengths (Å), bond angles (deg) and Hirshfeld atomic charges for $Q_2^3\,Q_2^2$, $Q_2^3\,Q_1^3\,Q_1^2\,Q_1^1$, and $Q_2^2\,Q_1^4\,Q_1^3\,Q_1^1$, optimized at the DF−BHL/DNP level of approximation.

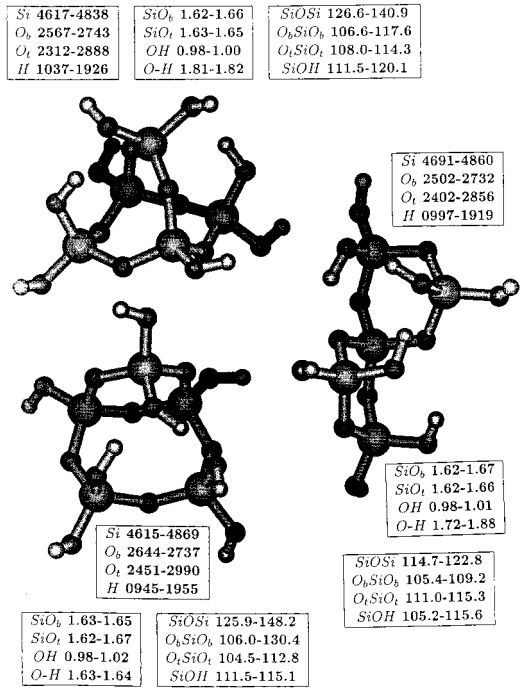

Figure 12. Bond lengths (Å), bond angles (deg), and Hirshfeld atomic charges for $Q_4^2\,Q_1^4$, $Q_2^2\,Q_2^3\,Q_1^2$e, and $Q_2^2\,Q_2^3\,Q_1^2$c, optimized at the DF−BHL/DNP level of approximation.

Å), as the two rings force the remaining hydroxyl groups too far apart to interact with each other. The condensation energy for this cluster is consequently positive and relatively high (+6.4 kcal mol^{-1}), making its formation very improbable, in agreement with experimental evidence.

The SiO bond length changes considerably in the constrained rings but is quite short in terminal groups (only 1.62−1.63 Å). Given the symmetry of the trimer−trimer framework, the SiOSi angles are all relatively similar for the three clusters (∼122−127°), except for the SiOSi angle in the edge common to both rings, which is much smaller but, again, almost constant (∼113°).

Central-Branched Trimer−Trimer Ring. The central-branched double-trimer ring (Figure 11, bottom left) results from the association of the four-silicon double ring with a monomer such that one silicon is bonded to four bridging oxygens. Both rings have chair conformations and are thus very similar to the four-silicon double ring but are more planar than the three-silicon ring.

There are two hydrogen bonds in this cluster, one of which is apparently overestimated. The small condensation energy for this cluster (−0.2 kcal mol^{-1}) is again due to the ring strain; in fact, the energy will be more positive because of the overestimated hydrogen bond. The corrected condensation energy of +3.1 kcal mol^{-1} is reasonable, though perhaps slightly too high when compared with the value obtained for the four-silicon double ring (+6.4 kcal mol^{-1}) without the lateral chain and a single hydrogen bond. The SiO distances in the rings are relatively large (1.64−1.68 Å) because of the ring strain, but the first SiO bond in the lateral chain is very strong: 1.61 Å. This bonding effect is confirmed by the observations made previously for all the trimer branched rings.

Outside-Branched Trimer−Trimer Ring. The outside-branched double-trimer ring (Figure 11, bottom right) differs from the previous cluster in that the monomer is attached to a silicon atom belonging to a single ring, forming a system with two hydrogen bonds, one of which is apparently too short (O···H = 1.75 Å).

The condensation energy (−2.1 kcal mol^{-1}) is slightly lower than for the previous clusters, which is as expected, because in the third cluster all silicon atoms are, at most, attached to three bridging oxygens, whereas in the second cluster a silicon atom was bonded to four bridging oxygens, thereby increasing the cluster strain. The corrected condensation energy (+1.2 kcal mol^{-1}) seems reasonable, given the strain accumulated in the double ring.

3.3.2. Double Rings: Corner-Bonded Double-Trimer Ring, Trimer−Tetramer Rings. The trimer−trimer double ring with the two rings bonded by a single silicon is discussed here, as are the two tetramer−trimer rings. Although relatively strained, both tetramer−trimer rings have been found in experimental work;[25,26] our calculations suggest that both clusters should be relatively stable.

Corner-Bonded Double-Trimer Ring. The corner-bonded, double-trimer ring, and the trimer−tetramer double rings, are shown in Figure 12. In the corner-bonded double-trimer ring (Figure 12, left), two three-silicon rings are attached to each other by a single silicon atom, instead of by a SiOSi edge, as in the three clusters before. The conformation proposed here is particularly favorable because it takes advantage of the "chair" conformation (the least-strained cyclic conformation) of both rings to allow the formation of four hydrogen bonds. Their formation should help considerably to stabilize the cluster.

The condensation energy obtained for this cluster (−1.6 kcal mol^{-1}) is reasonable, though one could expect this cluster to be significantly more stable than the two just considered, given the presence of four hydrogen

bonds and a single corner attachment instead of the shared edge between the two rings, which should decrease the strain. The corrected energy is, however, positive: +1.7 kcal mol^{-1}.

The SiO bond lengths change considerably in the double-ring framework (1.62−1.67 Å), essentially due to the different chemical environments seen by the central silicon atoms and the outer ones. The SiOSi angle has a surprisingly small range of variation (114.7−122.8°), considering that this is a highly strained cluster, where the environment of the central silicon atom (bonded to four bridging oxygens) differs from that of the other four (each bonded to only two bridging oxygens).

Edge-Bonded Trimer−Tetramer Ring. In the edge-bonded trimer−tetramer double ring (see Figure 12, bottom left), a four-silicon ring and a three-silicon ring share a common SiOSi chain, where a hydroxyl group in the three-silicon ring forms two hydrogen bonds with OH groups in the four-silicon ring, making the cluster even more rigid. The three-silicon and four-silicon rings keep the usual "chair" and "crown" conformations, but the two hydrogen bonds appear to be too short: 1.62−1.63 Å.

The bridging SiO_b bond length changes considerably (1.62−1.65 Å) in the three different silicon environments (Q_2^3, $Q_{2/3}^3$ and Q_1^2) present in the edge-bonded cluster. In the edge-bonded tetramer−trimer ring, the SiOSi bond angle is larger (148.2°) in the more-relaxed tetramer ring edge opposite the trimer ring than in the other cyclic bonds (125.9−130.4°).

The condensation energy obtained for this cluster, −13.6 kcal mol^{-1}, is probably too negative, even considering that this cluster is widely found in experimental sol−gel solutions. The corrected condensation energy, −7.0 kcal mol^{-1}, seems to be a more acceptable value for such a strained double ring.

Corner-Bonded Trimer−Tetramer Ring. The corner-bonded trimer−tetramer double ring (Figure 12, top left) differs from the above cluster in that the fragment containing the fifth silicon atom is bonded to two opposite corners of the four-silicon ring, instead of to two adjacent ones. In this different construction, the crown configuration of the tetramer ring becomes distorted, although two hydrogen bonds still form (O··· H = 1.81−1.82 Å).

In this cluster, each bridging oxygen forms a shorter bond (1.62−1.63 Å) and a longer one (1.65−1.66 Å). The Q_2^3 silicons belonging to both rings have two short and one long SiO_b bond lengths, while the other Q_2^2 bridging silicons have two long bonds and the fifth *Q* silicon has two short ones. The O_bSiO_b angles also change considerably (106.6−117.6°), which is surprising for such an hard angle. Because of the ring structure, the SiOSi angles change considerably, becoming smaller in the four-silicon ring (126.6−135.5°) than in the upper chain (see Figure 12) formed by the fifth silicon atom (136.3−140.9°).

The corresponding total condensation energy (−8.6 kcal mol^{-1}) is more than that for the edge-bonded ring described above, which is expected; forming the additional chain over the four-silicon ring should be energetically less favorable than forming a lateral three-silicon ring, as before. When corrected in the usual way, the energy is estimated as −2.0 kcal mol^{-1}, which is probably insufficiently negative in comparison with the double-trimer rings, which have almost the same energy and are much less commonly observed in experimental work.

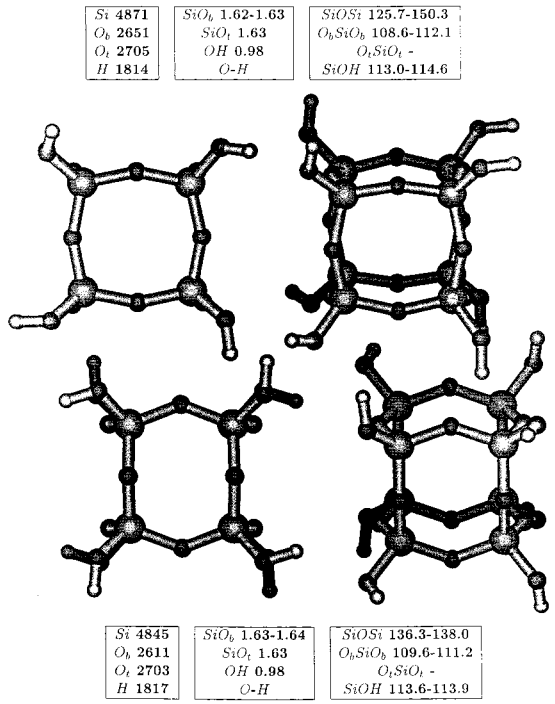

Figure 13. Bond lengths (Å), bond angles (deg), and Hirshfeld atomic charges for $Si_8O_{12}(OH)_8$ conformations, optimized at the DF−BHL/DNP level of approximation.

3.3.3. Complex Multiple Rings: Octamer Cage, Double-Hexamer Cage, and Sodalite Cage. In this section we report our analysis of the largest silica clusters studied so far: the 8-silicon, the 12-silicon, and the sodalite cages.

Octamer Cage. The most important conformations of the octamer cage are shown in Figure 13. In one conformation, the rings have a crown arrangement, as in the tetramer ring, while in the other they have a nonplanar hexagonal arrangement, where each oxygen is in the plane of one face of the cube and out of the plane of the face adjacent. Each ring in the cage defines a window that is almost circular in the crown arrangement (of dimensions 3.8 × 3.8 Å) and rectangular in the hexagonal arrangement (of dimensions 4.2 × 3.1 Å).

At the DF−BHL/DNP level of approximation, the "six-hexagon" conformation is +1.6 kcal mol^{-1} more stable than the "six-crown" conformation. If the hydroxyl groups are replaced by hydrogen atoms, the difference in energy between the two conformations decreases to only 0.5 kcal mol^{-1}. The condensation energy for $Si_8O_{12}(OH)_8$, although positive (+4.1 kcal mol^{-1}), is still less than the energy of a single hydrogen bond, which is reasonable for this relatively strained cluster. ^{29}Si NMR experimental evidence shows that this species is relatively stable in solution, at least for high pH values, though it has been found only in small concentrations.[21,25,26] The corresponding HF result of Hill and Sauer[33] for the crown conformation, −4.9 kcal per mole of SiO bonds, is surprising for such a constrained cage, which cannot form intramolecular hydrogen bonds.

Table 2. Condensation Energy (kcal mol^{-1}) for Optimized Silica Clusters[a]

		cal	cor	cal/*n*	cor/*n*	cal/*s*	cor/*s*
1 Si	Q_1^0	–	–	–	–	–	–
2 Si	Q_2^1	−9.4	−2.8	−9.4	−2.8	−4.7	−1.4
3 Si	$Q_2^1\,Q_1^2$	−18.5	−11.9	−9.3	−6.0	−6.2	−4.0
	Q_3^2	−1.6	−1.6	−0.5	−0.5	−0.5	−0.5
4 Si	$Q_2^2\,Q_2^1$	−38.2	−21.7	−12.7	−7.2	−9.5	−5.4
	$Q_3^1\,Q_1^3$	−30.6	−24.0	−10.2	−8.0	−7.7	−6.0
	$Q_2^2\,Q_1^3\,Q_1^1$	−6.0	−6.0	−1.5	−1.5	−1.5	−1.5
	$Q_2^3\,Q_2^2$	+6.4	+6.4	+1.3	+1.3	+1.6	+1.6
	Q_4^2	−25.7	−12.5	−6.4	−3.1	−6.4	−3.1
5 Si	$Q_3^2\,Q_2^1$	−43.6	−30.4	−10.9	−7.6	−8.7	−6.1
	$Q_3^1\,Q_1^3\,Q_1^2$	−40.2	−27.0	−10.1	−6.8	−8.0	−5.4
	$Q_4^1\,Q_1^4$	−32.0	−22.1	−8.0	−5.5	−6.4	−4.4
	$Q_2^2\,Q_1^3\,Q_1^2\,Q_1^1$	−11.0	−11.0	−2.2	−2.2	−2.2	−2.2
	$Q_2^2\,Q_2^1\,Q_1^4$	−11.3	−11.3	−2.3	−2.2	−2.2	−2.2
	$Q_2^3\,Q_2^1\,Q_1^2$cis	−11.0	−11.0	−2.2	−2.2	−2.2	−2.2
	$Q_2^3\,Q_2^1\,Q_1^2$trans	−10.5	−7.2	−2.1	−1.4	−2.1	−1.4
	$Q_2^3\,Q_1^3\,Q_1^2\,Q_1^1$	−2.1	+1.2	−0.4	−0.2	−0.4	−0.2
	$Q_2^2\,Q_1^4\,Q_1^3\,Q_1^1$	−0.2	+3.1	−0.0	+0.5	−0.0	+0.6
	$Q_4^2\,Q_1^4$	−1.6	+1.7	−0.3	+0.3	−0.3	+0.3
	$Q_3^2\,Q_1^3\,Q_1^1$	−31.0	−17.8	−6.2	−3.6	−6.2	−3.6
	$Q_2^2\,Q_2^3\,Q_1^2$e	−13.6	−7.0	−2.3	−1.2	−2.7	−1.4
	$Q_2^2\,Q_2^3\,Q_1^2$c	−8.6	−2.0	−1.4	−0.3	−1.7	−0.4
	Q_5^2	−25.2	−18.5	−5.0	−3.7	−5.0	−3.7
6 Si	Q_6^2	−48.7	−28.9	−8.1	−4.8	−8.1	−4.8
8 Si	Q_8^3	+4.1	+4.1	+0.3	+0.3	+0.5	+0.5

[a] Notes: cal = calculated; cor = corrected with 3.3 kcal mol^{-1} per hydrogen bond when O···H < 1.85 Å (see text); *n* = number of condensation reactions to form the cluster; *s* = number of silicons in the cluster.

Experimental OSiH, OSiO, and SiOSi bond angles for $Si_8O_{12}H_8$, (∼110−112°, 107−109°, and 149−154°) are reviewed by Bornhauser and Calzaferri.[47] Bond lengths are also given but change considerably in different studies.

3.4. Silica Clusters: Summary. Table 2 summarizes the calculated condensation energies discussed above. Overall, when we use corrected energies (i.e., values adjusted for the overestimation of the hydrogen bond strength by methodologies based on LDA), the qualitative agreement with experiment is satisfactory, in that the clusters with the larger (negative) condensation energies are observed in silicate solutions. As described in later sections, however, the condensation energies are satisfactorily modified by the effect of hydration, and a full account of the equilibrium distribution of silica clusters in solution will require these effects to be included in detail. Hydration will also modify the hydrogen bonding structure, the importance of which has been emphasized in the analysis just presented. Detailed knowledge of the structure and energetics in vacuo is, however, an essential prerequisite to understanding the properties of the clusters in solution.

3.5. Aluminosilicate Clusters. Although the majority of both computational and experimental studies have focused on silicate clusters, the properties and stabilities of aluminosilicate clusters are clearly of crucial importance. Indeed, a recent computational study[48] suggested that the energetics of small aluminosilicate clusters is an important influence on controlling Si/Al distribution in zeolites. In particular, DFT calculations show that the condensation of a silica monomer, $(Si(OH)_4)$, with an $[Al(OH)_4]^-$ monomer via the following reaction

$$Si(OH)_4 + [Al(OH)_4]^- \rightarrow [SiOAl(OH)_6]^- + H_2O \quad (1)$$

is energetically favorable by 27 kcal mol^{-1}, whereas the formation of Al−O−Al bridges by, for example,

$$2[Al(OH_4)]^- \rightarrow [Al_2O(OH)_6]^- + H_2O \quad (2)$$

is endothermic by 41 kcal mol^{-1}. Catlow et al.[48] therefore argued that the origin of Lowenstein's rule,[49] which forbids Al−O−Al bridges in zeolitic and related solids, is probably more associated with the energetics of the reactions involved in forming small clusters, particularly the unfavorable energetics of small clusters and rings containing Al−O−Al bridges, than with the energetics of the final aluminosilicate crystal structures.

4. Hydration Effects

All the calculations discussed earlier relate to clusters in vacuo. As noted, solvation will, of course, exert a crucial influence on the structures and stabilities of the clusters. Calculation of solvation energies however, is a very difficult problem in theoretical chemistry, and several different approaches for doing so are available, ranging from methods that treat the solvent as a continuum dielectric to methods in which the solvent is described explicitly,[8] but little attention has been paid to applying these techniques to studies of the interaction of silicate fragments with an aqueous environment. The problem of cluster hydration is addressed in this section through a variety of techniques. First we briefly

(47) Bornhauser, P.; Calzaferri, G. *Spectrochim. Acta* **1990**, *46A*, 1045.

(48) Catlow, C. R. A.; George, A. R.; Freeman, C. M. *J. Chem. Soc. Chem. Commun.* **1996**, 1311.

(49) Lowenstein, W. *Am. Miner.* **1954**, *39*, 92.

describe studies of the interaction of small numbers of water molecules with silicate species, using ab initio and combined MM/ab initio techniques. We then discuss efforts being made to describe the bulk effect of solvation on silicate fragments, using both ab initio and (more routinely) molecular mechanics methods.

4.1. Methods: Techniques and Previous Studies. Considerable attention has been paid to investigating the interaction of silicate species with small numbers of water molecules. The interaction of water molecules with SiOH can, in general, be of two types: The H_2O acts as a proton donor in a hydrogen bond to the oxygen atom of SiOH (type I), or the H_2O acts as a proton acceptor in a hydrogen bond to the hydrogen of SiOH (type II). Calculations using semiempirical methods have indicated that structures of type I are more stable than type II.[50] However, ab initio calculations, except for those at the STO-3G level, have suggested that the type II structures are more stable than those of type I. Ugliengo et al.[51] carried out calculations on the interaction of a water molecule with silanol (H_3-SiOH) as a model of the isolated hydroxyl of amorphous silica. Besides the type I and type II structures, they also investigated a bifurcated structure in which both hydrogen atoms of the water molecule interact with the oxygen atom in silanol. They confirmed that structure II is most stable; structure I has a nonplanar stable configuration, and the bifurcated type II structure is very weakly bound and unstable. Calculations with a 6−31G basis set give interaction energies of −36 kJ mol^{-1} for structure II,[52] which is in excellent agreement with the value estimated by Moravetski et al.,[35] −30 to −36 kJ mol^{-1}, for the average hydration of $Si(OH)_4$ per molecule of H_2O in neutral $H_4SiO_4 \cdot nH_2O$ complexes.

One method that can be used to model the effect of a solvent with ab initio (or even semiempirical) calculations is the COSMO method developed by Klamt and Schüürmann.[9] This method has been introduced into the ab initio DFT code DMOL by Andzelm et al.[53] The COSMO model is a continuum solvation model, in which the solute forms a cavity within the solvent of specified permittivity, represented by the dielectric continuum. The dielectric medium is polarized by the charge distribution of the solute, and the response of the dielectric medium is described by screening charges on the surface of the cavity.

The free energy of solvation ΔG can be calculated as

$$\Delta G = (E + \Delta G_{\text{nonelectrostatic}}) - E^0 \qquad (3)$$

where, E^0 is the total energy of the molecule in a vacuum and E is the total energy of the molecule in the solvent. $\Delta G_{\text{nonelectrostatic}}$ is the nonelectrostatic contribution from the dispersion and cavity formation effects, obtained by fitting the free energies of hydration for linear-chain alkanes as a function of surface area.[54] For polar, neutral molecules, the calculated hydration energies were in general within 2 kcal mol^{-1} of the experimental value after the nonelectrostatic contributions were taken into account. However, the agreement was less good for solute ions. Application of the technique to the problem of fragments in solution is discussed in greater detail below.

Another technique that can be used to estimate solvation energies is the so-called embedded cluster quantum mechanics (QM)/MM technique. Here the bulk solvent is modeled by using a MM force field, and the solute is modeled by QM methods. The interaction between the QM and MM regions can be modeled by using either mechanical embedding or electrostatic embedding. In mechanical embedding, the interactions between the QM and MM regions are modeled through a classical MM force field. In electrostatic embedding, the electrostatic potential attributable to the MM region is included in the QM Hamiltonian. For electrostatic embedding to be successful, the point charges included in the force field have to give a good description of the electrostatic potential; this is rare, however, since force fields are usually designed to give an accurate description of the total potential and not the individual components of the nonbonded potential. Nonetheless, electrostatic embedding allows polarization effects to be taken into account. Alternatively, polarization due to the environment can be accounted for using polarizable MM models. For QM/MM embedding techniques to be successful, the MM force field should be derived using calculations of approximately the same accuracy as those used for the QM region. One such method[55] incorporates solvation polarization by a classical fluctuating charge method, using molecular dynamics to treat the fluctuating charges as dynamical variables. This approach gave reasonable agreement with high-quality ab initio results for several dimers involving water. QM/MM techniques have also been used to study the interaction of water with a Brønsted acid site.[56] The binding energy of 79.4 kJ mol^{-1} for a water/$Si_2AlO_4H_9$ cluster, calculated by using a large basis set, was found to be in good agreement with a value calculated for the interaction of faujasite with water.[57]

4.2. Calculation of Solvation Energies Using the COSMO Methodology. We have used the ab initio DFT program DMOL together with the COSMO method to estimate the solvation energies for several small silicate fragments, shown in Figure 14. We used a DNP basis set at the BLYP level of approximation with a medium grid for integration.

The resulting solvation energies (Table 3) show a general trend for decreasing solvation energy with increasing silicon content. This is as expected, since the number of OH groups able to form hydrogen bonds with the water molecules decreases, a point that will be discussed in more detail later. The effect of the solvent on the structure is shown for the five-ring fragment in Figure 15. The structure in the gas phase is much more open than that in the solvent, and the orientation of the OH groups is different.

(50) Zhidomirov, G. M.; Kazansky, V. B. *Adv. Catal.* **1986**, *34*, 131.
(51) Ugliengo, P.; Saunders, V.; Garrone, E. *J. Phys. Chem.* **1990**, *94*, 2260.
(52) Chakoumakos, B. C.; Gibbs, G. V. *J. Phys. Chem.* **1986**, *90*, 996.
(53) Andzelm, J.; Kölmel, C.; Klamt, A. *J. Chem. Phys.* **1995**, *103*, 9312.
(54) Ben-Naim, A.; Marcus, Y. *J. Chem. Phys.* **1984**, *81*, 2016.
(55) Bryce, R. A.; Buesnel, R.; Hillier, I. H.; Burton, N. A. *Chem. Phys. Lett.* **1997**, *279*, 367.
(56) Sherwood, P.; de Vries, A. H.; Collins, S. J.; Greatbanks, S. P.; Burton, N. A.; Vincent, M. A.; Hillier, I. H. *J. Chem. Soc. Faraday Discuss.* **1997**, *106*, 79.
(57) Krossner, M.; Sauer, J. *J. Phys. Chem.* **1996**, *100*, 6199.

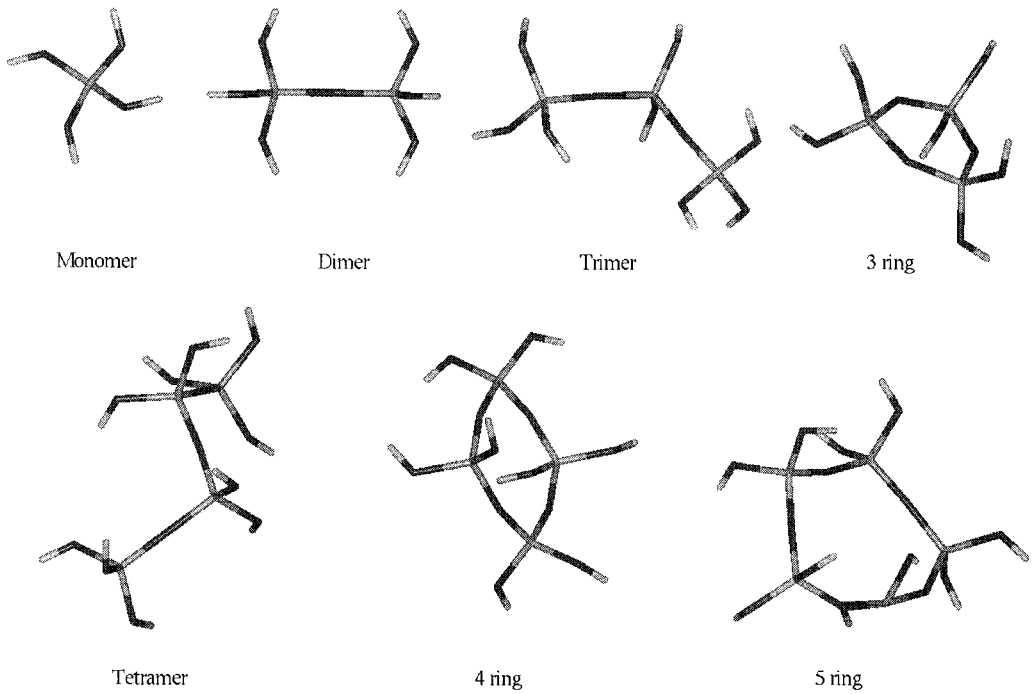

Figure 14. Silicate fragments used in DMOL/COSMO ab initio and cvff MM calculations of solvation energy.

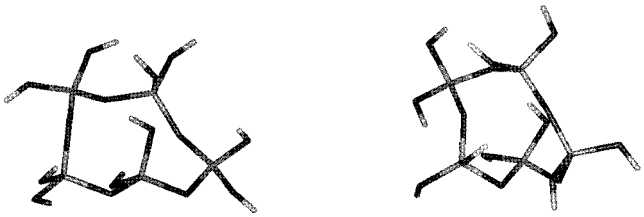

Figure 15. Comparison of gas-phase and DMOL/COSMO-optimized five-ring fragment.

Table 3. Solvation Energies (kcal mol^{-1}) per Silicon Calculated with DMOL/COSMO and cvff

structure	COSMO energy	MM energy	structure	COSMO energy	MM energy
monomer	−11.3	−11.1	tetramer	−8.6	−5.1
dimer	−11.1	−8.0	4-ring	−7.9	−2.6
trimer	−8.4	−6.2	5-ring	−5.4	−6.9
3-ring	−7.8	−7.5			

We also note that the DFT/COSMO methodology available in DMOL has been used recently to study the mechanism of condensation of silicate monomers to form a dimer species.[58] These calculations provided detailed information on the energetics of S_N2-like mechanisms and gave activation energies for these reactions in the region of 11−16 kcal mol^{-1}. These values accord well with those obtained in recent studies of zeolite nucleation using synchrotron radiation techniques.[59]

4.3. Molecular Mechanics Methods. By far the most widely used method of modeling silicate systems and their interactions is to use MM force fields. Such methods are widely used as they are efficient in terms of computer resources, and the force fields are parametrized for many different kinds of interactions. Both energy minimization (to obtain energy minima) and molecular dynamics techniques (to sample phase space) are widely employed. Since the energy calculated by use of an MM force field is a sum of bonding (representing the deviations for ideal bond lengths, bond angles, and torsion angles) and nonbonding (representing van der Waals and electrostatic interactions between nonbonded atoms) terms, it is not correct, strictly speaking, to compare calculated energies for different molecules because the "zero energy" calculated by MM will be different for different molecules. Comparisons of the energies of different conformations of the same molecule are, however, valid. In this section we describe recent work in which we used MM methods to understand the solvation of silicate systems in terms of the effect of fragment size and conformation on the calculated solvation energy.

When calculating solvation energies, one must construct an appropriate model for a solvated system. Here, there are two choices: either a model where the fragment is surrounded by a "droplet" of water, or a calculation based on periodic boundary conditions where the long-range electrostatic interactions in the solvent are taken into account. The solvation energy ΔE_{solv} can then by calculated by the following equation:

$$\Delta E_{solv} = E_{soln} - (E_{solv} + E_{frag}) \qquad (4)$$

where E_{soln} is the total energy of the solvent/solute system, E_{solv} is the energy of the solvent, and E_{frag} is the energy of the solute in the gas phase.

We calculated the solvation energies for the fragments in Figure 14 as follows. First, we solvated each fragment out to a distance of 15 Å, using the "soak" procedure in the INSIGHTII[12] modeling package, which places the solute in a "droplet" of water obtained from a molecular dynamics simulation of liquid water and removes the solvent molecules that overlap with atoms

(58) Pereira, J. C. G.; Price, G. D.; Catlow, C. R. A. *J. Chem. Soc., Chem. Commun.* 1998, 1387.
(59) Davies, A. T.; Sankar, G.; Catlow, C. R. A.; Clark, S. M. *J. Phys. Chem. B.* **1997**, *101*, 10115.

Table 4. Modified Charges in cvff Force Field[a]

atom type	Q (e)
Si	0.46
O	−0.29
H	0.175

[a] For the monomer $Si(OH)_4$ the above charges were used. For the other fragments, the same charges were used for O and H but the charge on Si was varied to ensure electroneutrality.

of the solute. We then minimized the total energy of the solute/solvent system, removed the solute, and repeated the minimization to obtain an energy for the pure solvent system. The solvation energy was then calculated according to eq 4. In several cases the solute/solvent system was subjected to dynamics, after which the minimization procedure was repeated. As noted earlier, we used dynamics to attempt to find the global energy minimum in the solvent/solute system.

The force field used was a variant of the standard cvff force field available in the DISCOVER code,[13] which we used to perform the energy minimization and molecular dynamics calculations. The modifications introduced improved the accuracy of the Si−O bond length determinations.[60] The charges used are shown in Table 4.

The calculated hydration energies in Table 3 show that the hydration energy per silicon decreases with increasing fragment size, a consequence of the decreasing number of OH groups available for hydrogen bonding with the water molecules for the larger fragments. Interestingly, in general, similar trends are found in the solvation energies calculated using the MM force field and those obtained by the ab initio DMOL/COSMO method.

Calculations to be discussed in greater detail later also explored solvation effects, using an alternative molecular mechanics potential, CFF91_czeo.[33,61] The hydration energies obtained are greater than those discussed above by a factor of 2−3. We consider the values to be discussed later significantly less reliable than those reported in this section for cvff calculations, which are in line with the results of the calculations performed with the COSMO technique. The CFF91_czeo force field may, however, yield more accurate structures for the silica fragments.

The sensitivity of the calculated hydration energies to the choice of interatomic potential parameters (particularly to the choice of charges) emphasizes the difficulty in obtaining definitive values for these important quantities. However, the energies reported in Table 3 represent, in our opinion, reasonable and useful estimates. They will be used in subsequent studies, in combination with the results in Table 2, to estimate the equilibrium distribution of clusters in solution.

5. Nucleation

The self-assembly of silica species in a gel into a crystalline solid is extremely difficult to study experimentally. Of particular interest is the initial assembly of what can become the crystallization nuclei; once such nuclei form, crystallization is rapid. NMR studies of gels are typically ex situ and offer little information once the fragments are larger than, say, 10 silicon atoms. Furthermore, once there is sufficient crystalline material to be identified by (in situ) diffraction techniques, the initial nucleation process is complete. SAXS/WAXS[62,63] and light-scattering methods[64] are capable of determining the size and, to a degree, the structure of the initial stages of crystallization and are now providing input into the understanding of the mechanism of such syntheses. However, they cannot provide atomic-level information on the structure, provide particle compositions, or be time-resolved on a reaction time scale.

Modeling methods can be used to construct possible crystallization precursors and to study their structure and interactions with solvent and other species such as templates. We summarize here our initial work[65] on understanding some of the processes involved in the formation of all-silica zeolite crystallization nuclei.

The approach we adopt here is complementary to those discussed in the previous section. Thus we have taken a typical zeolite structure, structure code LEV in this case, and deconstructed it to give us a range of silica structures that we might expect to form in the gel; these range from chains and simple ring structures to larger structures containing cages (Figure 16). We then performed energy minimization calculations on these structures in vacuo, in a solvent droplet, and in the presence of an organic template molecule (further details of the simulations are given elsewhere[65]). Unlike the work described in the previous section, we used the CFF91_czeo[33,61] MM potential, which generates more accurate zeolite structures although, as discussed earlier, the calculated hydration energies are probably too high.

5.1. Effect of Crystalline Field. We energy-minimized the fragments in the gas phase and compared the structures and energies with those for the fragments when constrained to their geometry in the crystal structure (i.e., we took the fragment from the crystal and optimized only the terminal OH groups). We found that all the gas-phase structures were more stable than those in the crystal, typically by ∼7 kcal mol^{-1} per Si atom (Table 5). In certain cases, for example, the eight-ring and multiple single-ring structures (such as a six-ring with two four rings attached), the gas-phase geometry is far removed from that in the crystal, as shown in Figure 17. However, more rigid fragments, such as double-six rings, do not undergo significant structural changes. A measure of the structural modification is given by the change in Connolly surface area[66] (Table 5). We conclude that the crystalline field provides added stability, allowing the individual components to take up geometries that are metastable with respect to the gas phase and must therefore be a driving force toward stabilizing these configurations. We also speculate that larger rings (such as 8-, 10-, and 12-

(60) Coombes, D. S.; Pereira, J. C. G.; Freeman, C. M.; Catlow, C. R. A.; Price, G. D., manuscript in preparation.
(61) Hagler, A. T.; Lifson, S.; Dauber, P. *J. Am. Chem. Soc.* **1979**, *101*, 5122.
(62) de Moor, P. P. E. A.; Beelen, T. P. M.; Komanschek, B. U.; Diat, O.; van Santen, R. A. *J. Phys. Chem. B* **1997**, *101*, 11077.
(63) Watson, J. N.; Iton, L. E.; Keir, R. I.; Thomas, J. C.; Dowling, T. L.; White, J. W. *J. Phys. Chem. B* **1997**, *101*, 10094.
(64) Schoeman, B. J. *Zeolites* **1997**, *18*, 97.
(65) Lewis, D. W.; Catlow, C. R. A.; Thomas, J. M. *J. Chem. Soc. Faraday Discuss.* **1997**, *106*, 451.
(66) Connolly, M. L. *Science* **1983**, *221*, 709.

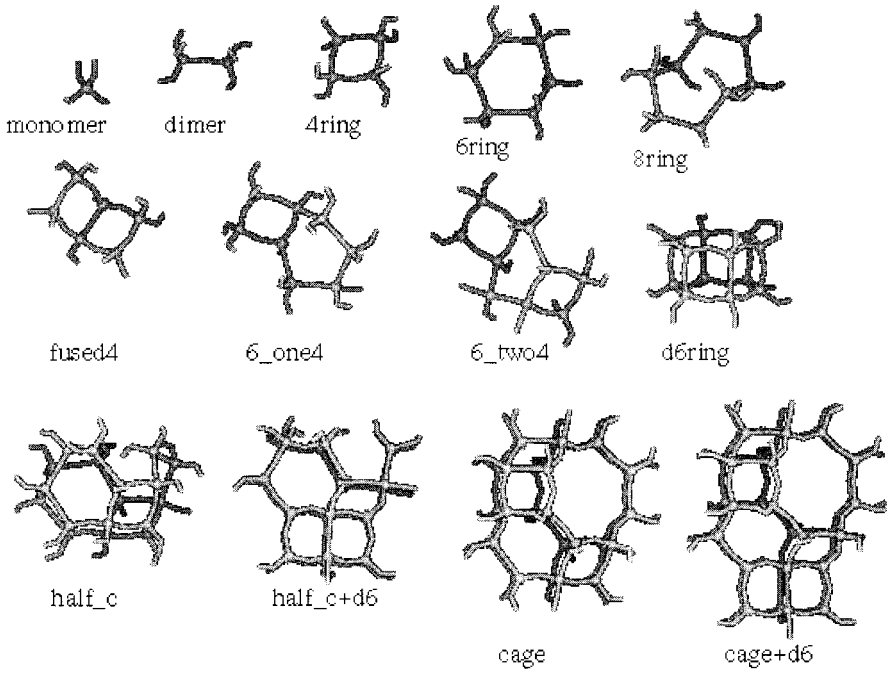

Figure 16. Silica clusters constructed from the LEV framework structure. Silicon atoms are shown as small spheres.

Table 5. Energy Differences (ΔE, kcal mol^{-1}) and Surface Area Changes (ΔSA, Å^2) between the Fragments in Their Gas Phase (gp), in Solvent (solv), and in Gas Phase in the Presence of the Template 1-Aminoadamantane (ADAMgp). Configurations with Respect to That in Their Crystalline Configuration (xtl)

	gp-xtl		solv-xtl		ADAMgp-xtl	
fragment	ΔE	ΔSA	ΔE	ΔSA	ΔE	ΔSA
monomer	−0.4	1.37	−0.2	2.4	−0.4	0.28
dimer	−11.9	0.65	−10.0	1.1	−2.8	−0.34
4-ring	−4.8	3.34	−4.4	0.1	−2.7	4.09
fused 4	−7.8	−1.29	−7.5	−2.4	−7.8	34.88
6-ring	−16.2	0.33	−16.2	−6.9	−2.2	0.58
6-one 4	−13.2	−0.70	−13.0	0.3	−13.1	−0.36
8-ring	−9.5	−0.11	−9.0	−1.6	−9.3	0.40
6-two 4	−11.1	−1.01	−11.0	−10.8	−11.0	−1.45
d6-ring	−2.1	−0.37	−1.9	−6.2	−2.0	−0.77
half-cage	−6.1	−0.12	−5.8	−6.2	−5.8	−0.09
half-cage+d6	−5.3	−0.58	−5.2	−4.3	−5.1	−0.39
cage	−7.7	−1.30	−7.5	0.4	−7.6	−1.44
cage+d6	−7.7	−2.09	−7.6	−2.9	−7.7	−1.88

rings), even if present as molecular species in the gel, will not be incorporated directly into a growing crystal surface because their geometries will be far removed from that which can be accommodated without significantly perturbing crystal growth. Therefore, such rings, when present in crystalline material, probably form as a consequence of the assembly of smaller fragments.

5.2. Effect of Solvent. By energy-minimizing the fragments in a droplet of water (as discussed above), we can not only obtain an estimate of the solvation energy but also observe the effect of the solvent on the structure of the fragments. The hydrophobic nature of the silica fragments results in changes in surface area upon solvation (Figure 18). In particular we noted changes in the concave surface area with respect to the total change in surface area (a concave area being an area in which a probe molecule would be in contact with three atoms of the surface[66]), clearly showing the hydrophobic nature of the inner surfaces of these clusters. Thus, large, open structures that are not made rigid by the interconnection of rings and cages will collapse inward, reducing their surface area (Figure 17). Conversely, the more-rigid units, which are self-supporting (such as the whole-cage fragment), maintain their surface area.

We also note that the self-energy of each of the fragments in solvent is now greater than the gas-phase energy (Table 5). Therefore, solvation drives the fragments to adopt geometries that are considerably different from the gas-phase structures.

5.3. Effect of Template. Organic cations added to the synthesis gels are well-known to have a "templating," or structure-directing, effect. Previous modeling studies, by us[67−69] and others,[70,71] that demonstrated an energetic rationalization for the templating effect have considered only the template−framework interactions once crystallization is complete. But what effect do templates have on the structure of precrystallization species?

We calculated the equilibrium geometries of the silica clusters in the presence of two organic species that form the parent zeolite structure, namely, 1-aminoadamantane and *N*-methylquinuclidinium. Figure 19 compares the changes in surface area from the crystal geometry with and without template. Clearly the presence of the template reduces the collapse of the more open fragments, which we commented on in Section 5.2; however, the template also affects the intramolecular energy of the fragment (Table 5). The presence of the template raises the self-energy of the fragments closer to the energy found in the crystalline configuration. Thus, the template provides a further driving force, similar to that

(67) Lewis, D. W.; Freeman, C. M.; Catlow, C. R. A. *J. Phys. Chem.* **1995**, *99*, 11194.
(68) Lewis, D. W.; Catlow, C. R. A.; Thomas, J. M. *Chem. Mater.* **1996**, *8*, 1112.
(69) Bell, R. G.; Lewis, D. W.; Voigt, P.; Freeman, C. M.; Thomas, J. M.; Catlow, C. R. A. *Stud. Surf. Sci. Catal.* **1994**, *84*, 2075.
(70) Harris, T. V.; Zones, S. I. *Stud. Surf. Sci. Catal.* **1994**, *84*, 29.
(71) Stevens, A. P.; Gorman, A. H.; Freeman, C. M.; Cox, P. A. *J. Chem. Soc. Faraday Trans.* **1996**, *92*, 2065.

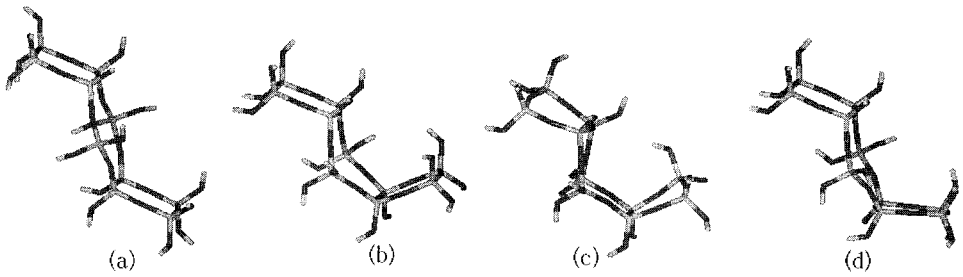

Figure 17. Geometric changes in different environments for the 6_two4 fragment, a single six-ring with a four-ring fused at either end (see Figure 16): (a) geometry in the crystalline environment, (b) gas-phase structure, (c) in solvent, and (d) in solvent and in the presence of the organic template 1-aminoadamantane.

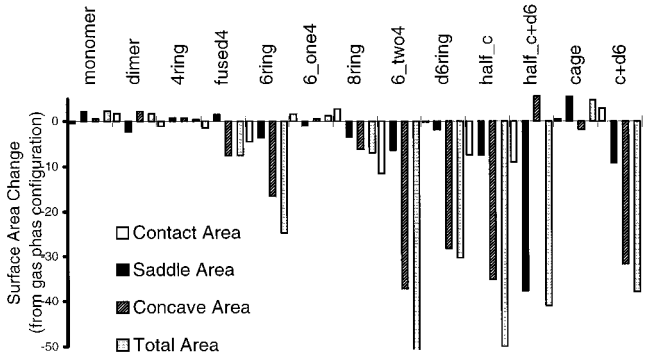

Figure 18. Changes in water-accessible surface area (Å^2) of the fragments on solvation relative to the surface area in the gas-phase configuration.

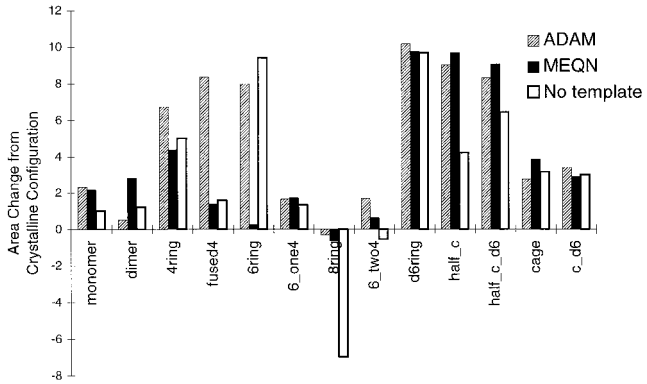

Figure 19. Change in surface area (Å^2) from the crystalline configuration to the gas-phase configuration, in the presence and absence of the templates ADAM (1-aminoadamantane) and MEQN (*N*-methylquinuclidinium).

seen in solvation (discussed above), by which the inorganic species can be stabilized to allow the formation of the metastable crystalline structure.

5.4. Interactions in the Gel: Template and Solvation Effects. A gel from which a zeolite will form does, of course, contain both silica fragments and templates as well as the solvent. Therefore, we have determined the combined effects of solvation and template on our model fragments by energy-minimizing the fragment−template complexes in the same solvent droplet as above. We now gain an understanding of how the template−fragment interactions stabilize the fragment. The main effect of solvent, as discussed above, is to cause collapse of the open structure of the fragments through the hydrophobic nature of the silica surface. However, the presence of the template shields the fragment from the solvent and therefore prevents this collapse. This effect can be illustrated by comparing the change in surface area (from the crystalline configuration) upon solvation, with and without the presence of a template (Figure 20). As expected, the effect is more dramatic for those structures that have cavities, such as the half-cage fragments, where the hydrophobic regions of the fragment are more exposed. However, these calculations also demonstrate that the binding energy of the template−fragment complex (i.e., the energy gained by bringing the fragment and template into close contact) is reduced on solvation, which suggests that the shielding effect does not fully compensate for the loss of solvation of the template. Furthermore, such fragment−template complexes may not be stable over the time scales required for the fragment to grow.

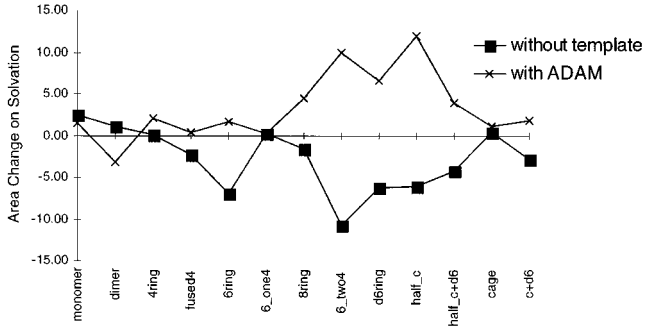

Figure 20. Effect of the template, 1-aminoadamantane (ADAM), on the surface area (Å^2) of the solvated fragments.

5.5. Dynamic Stability of Template−Fragment Complexes. If growth of these fragments into larger crystallization nuclei occurs by the condensation of monomers, small fragments, or both around the template, then the template−fragment complexes must be stable in an aqueous environment. In particular, the complexes must remain bound for a sufficient period to permit condensation of further silica species with the fragment. To investigate the stability of solvated silica species and a typical template, tetramethylammonium, we performed molecular dynamics simulations to observe the evolution of the complex with time. For neutral silica fragments, we found that, over a relatively short time, ∼50 ps, the complex dissociated (shown schematically in Figure 21). However, if charged silica species were considered, for example, $Si(OH)_3O^-$ and $(OH)_3Si-O-Si(OH)_2O^-$, this dissociation was reduced. From these simple calculations, therefore, we conclude that long-range Coulombic interactions are critical in maintaining contact between the organic and inorganic components of the synthesis gel.

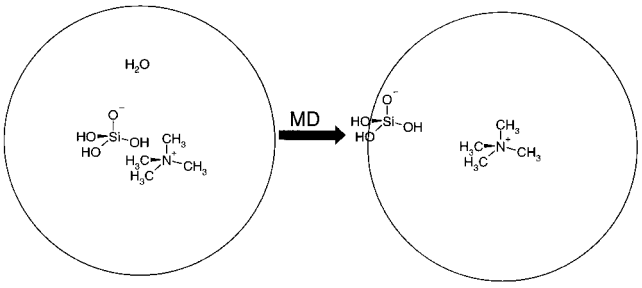

Figure 21. Schematic representation of the molecular dynamics (MD) simulations of template and fragment complexes in water; over time, the fragments and template dissociate.

5.6. Discussion of Nucleation. From these exploratory calculations, several qualitative conclusions can be drawn about the roles of the various gel components. First, clusters of framework material require some form of stabilization to maintain their structure under the influence of water; template species provide this stabilization. Solvation of the hydrophobic regions of the silica clusters results in the collapse of the open structure of the fragments that can be expected to be present during the early stages of crystal growth. The role of the template here is to shield the hydrophobic regions from the solvent and thus maintain the open structure. This observation is consistent with the proposal that nuclei grow initially through replacing the solvent surrounding a template species by silica fragments, which condense.[72−75]

Second, Coulombic interactions are essential to allow the template−fragment complex to remain bound over a time scale that allows for further condensation onto the fragment. We have found that only when the silica fragments are charged (i.e., have undergone some degree of deprotonation) are fragment−template complexes stable, a finding that may provide some insight into the relatively long induction periods noted in zeolite synthesis; neutral monomeric species must first either polymerize or deprotonate before the enthalpic driving force provided by interactions with the template results in the beginnings of nucleation.

In these calculations, we have considered only organic species as templating agents. However, alkali metal cations are the most common additive in zeolite preparations and are present at high concentrations in natural zeolites. Do they have a templating effect? We consider this likely. The two effects discussed above—the shielding of water−silica surface interactions and the binding of complexes—can readily be applied to metal cations. The water in the solvation shell of a metal cation can be considered ordered and furthermore will not have the same charge distribution as bulk water. Thus we can envisage that the cation and its solvation shell act in much the same way as an organic cation. For example, in the natural Levyne structure, the cage is occupied by a $Ca(H_2O)_6^{2+}$ species, for which the van der Waals volume is very similar to that of the templates used to form the synthetic materials with the same structure.

Much more work is needed on the problems explored above. However, the calculations we have reported provide a useful basis for future computational studies of zeolite nucleation and the role of solvation and templating.

6. Summary and Conclusions

The computational studies summarized in this paper are the first stage in providing a firmer basis for the development of atomistic models of hydrothermal synthesis. We have established accurate geometries for key silica fragments in vacuo; condensation energies for the formation of the species from silica monomers have also been calculated. The difficult problem of calculating hydration energies has also been investigated: the agreement between the energies obtained by MM and QM methods suggests that the values obtained are reasonable estimates. Finally, our calculations have highlighted the importance of template−fragment interactions in solution and the importance of Coulombic effects in binding template−fragment nuclei. Future studies will extend the calculations to consider charged clusters and will develop both thermodynamic models for the equilibrium concentration of clusters in solution and kinetic models for their condensation into microporous and related structures.

Acknowledgment. We are grateful to C.M. Freeman (Molecular Simulations Inc.) and G.D. Price (University College London) for many useful discussions. Molecular Simulations Inc. is gratefully acknowledged for provision of software and for partial support of this work. We also thank EPSRC and NERC for supporting this work. D.W.L. thanks the University of Cambridge for the award of an Oppenheimer Fellowship and the Royal Society for additional funding.

CM980302O

(72) Burkett, S. L.; Davis, M. E. *J. Phys. Chem.* **1994**, *98*, 4647.
(73) Burkett, S. L.; Davis, M. E. *Chem. Mater.* **1995**, *7*, 1453.
(74) Burkett, S. L.; Davis, M. E. *Chem. Mater.* **1995**, *7*, 920.
(75) Cox, P. A.; Casci, J. L.; Stevens, A. P. *J. Chem. Soc. Faraday Discuss.* **1997**, *106*, 473.